

## RESEARCH ARTICLES

one mouse (Fig. 1D), to other retinal layers in another mouse (32).

Finally, it is worth considering aire-deficient mice as a model of APECED. Like human patients, the murine model shows multiorgan attack by lymphocytic infiltrates and recognition by serum autoantibodies. In both cases, there is disease heterogeneity between individuals and exacerbation with age. The differences between humans and mice in the spectrum of organs targeted could well be due to the influence of genetic modifiers, as recently described for the HLA locus in humans (39). Aire-deficient mice should prove invaluable for dissecting the relative importance of genetic, environmental, and stochastic processes in determining the target organ specificity of autoimmune destruction.

### References and Notes

1. K. M. Garza, V. S. Chan, P. S. Ohashi, *Rev. Immunogenet.* **2**, 2 (2000).
2. D. Hanahan, *Curr. Opin. Immunol.* **10**, 656 (1998).
3. L. Klein, B. Kyewski, *Curr. Opin. Immunol.* **12**, 179 (2000).
4. J. Derbinski, A. Schulte, B. Kyewski, L. Klein, *Nature Immunol.* **2**, 1032 (2001).
5. L. Klein, B. Roettinger, B. Kyewski, *Eur. J. Immunol.* **31**, 2476 (2001).
6. P. Naquet, M. Naspetti, R. Boyd, *Semin. Immunol.* **11**, 47 (1999).
7. H. Kishimoto, J. Sprent, *Clin. Immunol.* **95**, S3 (2000).
8. C. Jolicœur, D. Hanahan, K. M. Smith, *Proc. Natl. Acad. Sci. U.S.A.* **91**, 6707 (1994).
9. K. M. Smith, D. C. Olson, R. Hirose, D. Hanahan, *Int. Immunol.* **9**, 1355 (1997).
10. M. W. Hoffmann, J. Allison, J. F. Miller, *Proc. Natl. Acad. Sci. U.S.A.* **89**, 2526 (1992).
11. M. W. Hoffmann, W. R. Heath, D. Ruschmeyer, J. F. A. P. Miller, *Proc. Natl. Acad. Sci. U.S.A.* **92**, 9851 (1995).
12. M. G. Von Herrath, J. Dockter, M. B. A. Oldstone, *Immunity* **1**, 231 (1994).
13. A. M. Sponaas *et al.*, *Int. Immunol.* **6**, 277 (1994).
14. S. J. Antonia, T. Geiger, J. Miller, R. A. Flavell, *Int. Immunol.* **7**, 715 (1995).
15. M. Oukka, M. Cohen-Tannoudji, Y. Tanaka, C. Babinet, K. Kosmatopoulos, *J. Immunol.* **156**, 968 (1996).
16. L. Klein, T. Klein, U. Ruther, B. Kyewski, *J. Exp. Med.* **188**, 5 (1998).
17. M. Oukka *et al.*, *Immunity* **4**, 545 (1996).
18. L. Klein, M. Klugmann, K.-A. Nave, V. K. Tuohy, B. Kyewski, *Nature Med.* **6**, 56 (2000).
19. A. C. Anderson *et al.*, *J. Exp. Med.* **5**, 761 (2000).
20. A. Pugliese *et al.*, *Nature Genet.* **15**, 293 (1997).
21. P. Vafiadis *et al.*, *Nature Genet.* **15**, 289 (1997).
22. C. E. Egwuagu, P. Charukamnoetkanok, I. Gery, *J. Immunol.* **159**, 3109 (1997).
23. P. Bjorses, J. Aaltonen, N. Horelli-Kuitunen, M. L. Yaspo, L. Peltonen, *Hum. Mol. Genet.* **7**, 1547 (1998).
24. P. Peterson *et al.*, *Immunol. Today* **19**, 384 (1998).
25. P. G. Kumar *et al.*, *J. Biol. Chem.* **276**, 41357 (2001).
26. J. Pitkanen *et al.*, *J. Biol. Chem.* **275**, 16802 (2000).
27. P. Bjorses *et al.*, *Am. J. Hum. Genet.* **66**, 378 (2000).
28. M. C. Rosatelli *et al.*, *Hum. Genet.* **103**, 428 (1998).
29. S. Zuklys *et al.*, *J. Immunol.* **165**, 1976 (2000).
30. C. Ramsey *et al.*, *Hum. Mol. Genet.* **11**, 397 (2002).
31. See supporting data on Science Online.
32. M. S. Anderson *et al.*, data not shown.
33. K. Nagamine *et al.*, *Nature Genet.* **17**, 399 (1997).
34. M. Halonen *et al.*, *J. Histochem. Cytochem.* **49**, 197 (2001).
35. M. Heino *et al.*, *Biochem. Biophys. Res. Commun.* **257**, 821 (1999).
36. M. Heino *et al.*, *Eur. J. Immunol.* **30**, 1884 (2000).
37. M. Gylling *et al.*, *J. Clin. Endocrinol. Metab.* **85**, 4434 (2000).
38. A. Kojima, R. T. Prehn, *Immunogenetics* **14**, 15 (1981).
39. M. Halonen *et al.*, *J. Clin. Endocrinol. Metab.* **87**, 2568 (2002).

40. We thank G. Losyev, Q.-M. Pham, J. Rasmussen, and R. Saccone for help with flow cytometry, mice, microarray software and chip analysis, respectively, and E. Smith for assistance with the figures. Supported by the W. T. Young Chair fund, NIH grant RO1 DK60027-01 (D.M. and C.B.), Joslin Diabetes Center grant DERC 2 P30 DK36836-16, a Howard Hughes Medical Institute Postdoctoral Fellowship for Physicians and NIH grant KO8-DK59958-01A1 (M.S.A.), an NSF Graduate Research Fellowship and NIH training grant 2T32 DK07260-26 to Joslin Diabetes Center (E.S.V.), Irvington Institute for Immunological Research (L.K.), Juvenile Diabetes Research Foundation (Z.C.), Human Frontier Science Program (S.B.), and an NRSA fellowship in Cancer Immunology (T32CA70083-05) and the Cancer Research Institute (S.J.T.).

### Supporting Online Material

www.sciencemag.org/cgi/content/full/1075958/DC1

Materials and Methods

Figs. S1 to S8

References

10 July 2002; accepted 19 September 2002

Published online 10 October 2002;

10.1126/science.1075958

Include this information when citing this paper.

## REPORTS

# Broadband Modulation of Light by Using an Electro-Optic Polymer

Mark Lee,\* Howard E. Katz, Christoph Erben, Douglas M. Gill, Padma Gopalan, Joerg D. Heber, David J. McGee

A major challenge to increasing bandwidth in optical telecommunications is to encode electronic signals onto a lightwave carrier by modulating the light up to very fast rates. Polymer electro-optic materials have the necessary properties to function in photonic devices beyond the 40-GHz bandwidth currently available. An appropriate choice of polymers is shown to effectively eliminate the factors contributing to an optical modulator's decay in the high-frequency response. The resulting device modulates light with a bandwidth of 150 to 200 GHz and produces detectable modulation signal at 1.6 THz. These rates are faster than anticipated bandwidth requirements for the foreseeable future.

Transmitting signals by using infrared light through optical fiber is the most effective way to move large amounts of data rapidly over long distances. Consequently, optical communications form the backbone of the Internet and telephone networks, and they are envisioned to carry real-time multimedia content in the future.

Bell Laboratories—Lucent Technologies, 600 Mountain Avenue, Murray Hill, NJ 07974, USA.

\*To whom correspondence should be addressed, E-mail: markl@lucent.com

Approaches to increasing optical bandwidth are being pursued to accommodate anticipated growth in data traffic. At present, high-speed optical networks use bandwidths of 10 GHz (~10 billion bits per second) per channel, and 40-GHz products are being introduced. Basic research efforts are aiming to push bandwidths to 80, 100, and even 160 GHz.

Expanding bandwidth beyond 100 GHz involves many scientific and engineering challenges, among which is the encoding of electronic data signals onto a lightwave carrier by

modulating the light in phase or amplitude. This is usually done with an electro-optic (E-O) modulator ( $I$ ), where a signal voltage changes the refractive index of an E-O dielectric optical waveguide, modulating the phase of a guided lightwave. Amplitude modulation is obtained by generating a phase difference  $\Delta\Phi$  between light in two coherent waveguides and then combining to produce constructive or destructive interference. In present technology, lithium niobate is the E-O material most widely used in high-speed optical modulators.

An E-O device produces the strongest modulation when  $\Delta\Phi = \pi$  radians. For an input voltage  $V_{in}$ ,  $\Delta\Phi \propto \pi(V_{in}/V_{\pi})$ , where  $V_{\pi}$  is the "half-wave" voltage that makes  $\Delta\Phi = \pi$  near zero frequency [direct current (dc)], is:

$$V_{\pi} = \frac{\lambda_0 d}{2n_{opt}^3 r \Gamma L} \quad (1)$$

where  $\lambda_0$  is the carrier wavelength,  $d$  is the gap between voltage electrodes,  $n_{opt}$  is the optical refraction index,  $r$  is the E-O coefficient of the dielectric,  $L$  is the device length, and  $\Gamma$  is defined as the signal electric field in the optical waveguide normalized to the field that would be there if air were the dielectric. The central problem for high-speed operation is that, for a fixed  $V_{in}$ ,  $\Delta\Phi$  decreases as modulation frequency increases. This response deterioration has three physical origins. The first is dissipation of  $V_{in}$  due to resistance in the electrodes guid-

ing the voltage signal. At frequencies ( $f$ ) that are high,  $\Delta\Phi$  falls as  $1/L(\rho f)^{1/2}$ , where  $\rho$  is the electrode resistivity.  $V_{\pi}$  is also diminished by absorption in the optical waveguide dielectric, which causes  $\Delta\Phi$  to drop as  $1/fL\tan\delta$ , where  $\tan\delta$  is the loss tangent. Finally, a velocity mismatch between signal and carrier waves causes  $\Delta\Phi$  to roll off as  $\sin(fL\Delta n)/(fL\Delta n)$ , where  $\Delta n$  is the refraction index difference between the guided signal and optical modes.

Degradation of the high-frequency response can be reduced to some extent by making  $V_{\pi}$  lower without increasing  $L$  (2). Experimental modulators have achieved  $V_{\pi} \approx 1$  V (3, 4), compared with the 3 to 5 V in commercial devices. However, very broad bandwidth performance requires minimizing the loss parameters  $\rho$ ,  $\tan\delta$ , and  $\Delta n$ . For lithium niobate, there are strong doubts about its usefulness above 100 GHz, where its intrinsically high values of  $\tan\delta$  and  $\Delta n$  will rapidly decrease response to unacceptably low levels (5).

Polymeric materials have recently ignited interest for use in high-speed photonics. A record low  $V_{\pi} = 0.8$  V was demonstrated (4) by means of a chromophore that generates a large  $r \sim 60$  pm/V (6, 7). In addition, the dielectric properties of many polymers are suitable for high-frequency applications. Millimeter-wave measurements on several polymers show very low  $\tan\delta$  values and refractive indices that are not dispersive and within 10% of optical indices (8). Nevertheless, it has still proven difficult to fabricate very broad bandwidth modulators. The fastest polymer modulators reported show bandwidths (9) of 30 to 40 GHz (10, 11), although a signal remains observable to 113 GHz (12). Up to now, polymer modulators have not exceeded the fastest experimental lithium niobate designs that have 70- to 105-GHz bandwidths (13).

We show that, by characterizing and selecting an appropriate combination of materials, the favorable properties of polymers can be exploited to essentially eliminate all dielectric factors degrading high-frequency response. Thus the bandwidth of a polymer modulator need not be limited by any intrinsic property of the polymers. The basic design of the modulator is a 2-cm-long push-pull Mach-Zehnder interferometer similar to what is analyzed extensively in the literature (4, 10, 12, 15, 16) (see Fig. 1). The commercially available chromophore disperse red-1 (DR1) bonded in a polymethylmethacrylate (PMMA) host is used as the E-O active optical core, which is sandwiched between glass resin claddings. A ridge optical waveguide etched into the core has a guided mode optical index  $n_{\text{opt}} = 1.54$ . Details of the modulator materials and construction are specified separately (14).

The polymer stack is also the spacer for a gold microstrip that guides the modulation voltage signal. The choice of core and cladding

materials based on their high-frequency dielectric properties is critical. First, the polymers have very low  $\tan\delta$ ,  $\sim 10^{-4}$  up to 400 GHz (8). Thus dielectric loss is insignificant compared with other loss mechanisms such as electrode resistance. Second, the signal frequency dielectric constant ( $\epsilon$ ) of the composite polymer is 2.8 (8). It is crucial that  $\epsilon^{1/2} > n_{\text{opt}}$  to achieve a velocity match between guided mode signal and optical waves, because the index  $n_m$  of a modulation signal guided by the microstrip can only be made smaller than  $\epsilon^{1/2}$ . Thus, with  $\epsilon^{1/2} = 1.67$ , it is possible to engineer the microstrip to make  $n_m = n_{\text{opt}} = 1.54$  to within experimental accuracy. This eliminates the  $\Delta n$  factor in the response decay. Finally, the microwave dielectric constant of the PMMA + DR1 is  $\epsilon_{\text{core}} = 2.3$ , compared with  $\epsilon_{\text{clad}} = 2.9$  for the glass resin, the reverse of the optical index contrast. Because  $\epsilon_{\text{core}} < \epsilon_{\text{clad}}$ , a voltage  $V$  applied to the microstrip gives an electric field in the core greater than in the cladding and greater than the field  $V/d$  for an air gap between electrodes. Thus  $\Gamma$  in Eq. 1 can exceed unity. Electrostatic modeling shows that with our materials  $\Gamma = 1.2 \pm 0.1$ , compared with  $\Gamma \approx 0.3$  for lithium niobate modulators and  $\Gamma \approx 0.8$  for polymer modulators with  $\epsilon_{\text{core}} > \epsilon_{\text{clad}}$ .

We measured the basic characteristics of the modulator (Fig. 2) at 1310-nm carrier wavelength and detected the modulated light output using a photodiode. The input voltage was ramped at 24 V/ms, with the microstrip termi-

nated by a matched impedance. The inset shows the sinusoidal transfer characteristic of an E-O modulator. The figure shows the same data on a decibel (dB) scale. The voltage difference between maximum and minimum optical intensity gives  $V_{\pi} = 11.3$  V. This is consistent with a product  $r\Gamma$  of 5 to 8 pm/V. The extinction ratio  $X$  is defined as the ratio of the maximum to minimum intensities in the modulated light. A larger value of  $X$  means the signal has better signal-to-noise properties. A voltage  $V_{\pi}$  gives  $X = 20.7$  dB, which is a useful value.

Then, we measured the response to high-frequency modulation using sideband detection. When an optical carrier at frequency  $f_c$  is amplitude modulated (AM) by a sinusoidal signal at frequency  $f_m \ll f_c$ , the optical power spectrum of the AM light consists of a main peak at wavelength  $\lambda_c = c/f_c$ , where  $c$  is the speed of light, plus two sideband peaks at wavelengths  $\lambda_c(1 \pm \delta f/f_c)$ , where  $\delta f = f_c - f_m$ . These sidebands carry the data signal. The sideband power  $P_{\text{SB}}$  relative to the carrier power  $P_c$  is  $P_{\text{SB}}/P_c = 1/4(1 - X^{-1/2})^2$ . As  $X$  increases,  $P_{\text{SB}}/P_c$  also increases but never exceeds  $1/4$  even for an ideal  $X \rightarrow \infty$ .

Optical spectra of the AM light from the modulator are shown in Fig. 3. A 6-V dc bias was maintained to operate the modulator in its linear response regime (Fig. 2, inset). The sideband wavelengths are plotted relative to the carrier, which defines zero wavelength shift and reference power  $P_c = -15$  dBm. At all frequen-

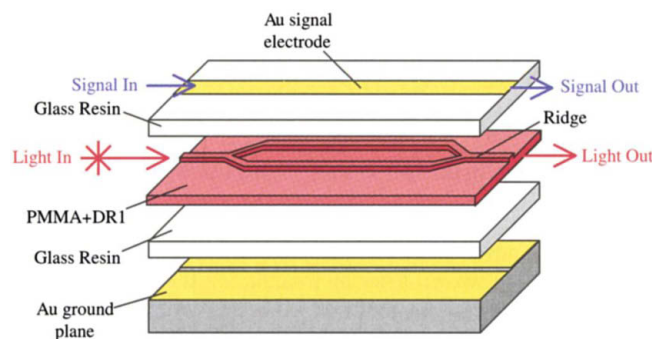


**Fig. 1.** Schematic of the polymer modulator layers. The polymer layers are spun on at 1 to 2 krpm and cured up to 200°C. The two arms of the ridge waveguide are separated by a 8- $\mu\text{m}$  gap. The top electrode is 30  $\mu\text{m}$  wide.

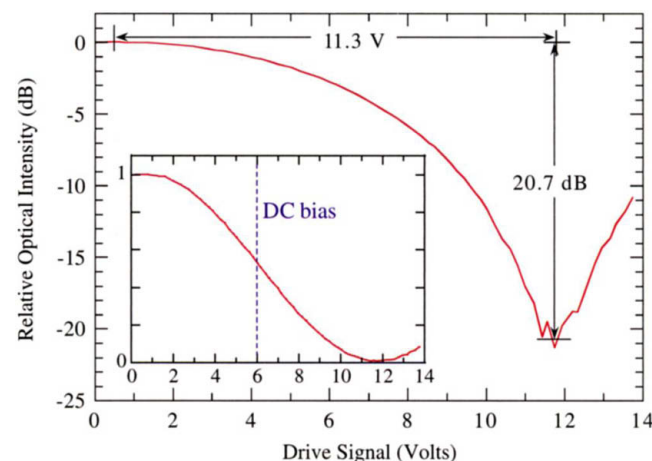


**Fig. 2.** Basic characteristics of the modulator. The inset shows the electric-to-optical transfer characteristic. The dashed line indicates the modulator's linear response regime. The main figure shows the same data plotted on a decibel scale.  $V_{\pi}$  and  $X$  are indicated.

## REPORTS

cies, the signal power was adjusted so that a 1-V peak amplitude appeared at the microstrip input, which was the largest voltage that could be applied across the entire frequency range. This allows the relative heights of the sidebands to be compared directly. The inset shows microwave sidebands at several modulation frequencies to 25 GHz. The main figure shows sidebands at modulation frequencies from 25 to 145 GHz. Details of the high-frequency measurement methods are described separately (14).

One obvious feature of the data is that the sidebands decrease little as frequency increases. The 25-GHz sideband is within ~0.5 dB of a reference sideband measured at 10 MHz. From 25 to 145 GHz, the sidebands drop less than 3 dB. This gradual response decay is quantified in Fig. 4. The relative optical response plotted is the sideband power normalized to the power at a relatively low frequency, in this case, 10 MHz. Except at a few resonant dropouts, the optical response remains flat to within 0.5 dB up to ~20 GHz, at which point it begins to fall. However, even at 145 GHz the response decreases only by about -2.5 dB. The right side electrical response is commonly used in engineering and equals the square root of the optical response (see supporting online text).

To understand the performance better, we modeled the response using a Sonnet electromagnetic simulator. If we assume no dielectric losses and use a gold conductivity of  $3.7$  to  $4.1 \times 10^7$  mhos/m, we found good agreement with the data at high frequencies, namely, 20 to 145 GHz. The simulation calculated a voltage attenuation of  $0.25$  dB/cm/GHz<sup>1/2</sup> leading to a 1.8-dB response drop, compared with the ~2 dB measured. This supports the claim that the effects of dielectric loss and velocity mismatch are negligible. To estimate the -3-dB bandwidth from the data, the electrode surface resistance loss is extrapolated from the highest frequency data points to obtain a best-estimate of 185 GHz. Extrapolations that fall reasonably within the error bars place the bandwidth between 150 and 205 GHz. At low frequencies, there is some discrepancy between model and data. Sonnet shows a 1.6-dB drop from 10 MHz to 20 GHz, in contrast to the ~0.5-dB drop measured. Including this drop, the modeled bandwidth would be around 115 GHz. We are currently trying to understand the physical reason behind the 1-dB difference between modeling and data at low frequencies. Nonetheless, the results for high frequencies clearly demonstrate that the bandwidth

is determined by the gold surface resistance.

If electrode surface resistance dominates the high-frequency roll-off, then the response degrades slowly enough to operate conceivably well above the -3-dB point. As a demonstration, we drove this modulator at 1.6 THz using a molecular gas laser. The resulting optical spectrum is shown in the inset, Fig. 4. The 1.6-THz sidebands are small but have 3 to 4 dB of signal-to-noise ratio. However, because the actual power coupled from the laser to the modulator could not be reliably determined, the 1.6-THz response is not included in the main part of Fig. 4.

The ability to support extremely broad bandwidth operation, together with the possibility of low operating voltages, makes it plausible that an ultrafast polymer modulator with truly practical characteristics can be fabricated in the near future. In addition, the fabrication methods for polymer devices offer opportunities for cost reduction relative to more common E-O materials. Although questions about the long-term reliability of polymer devices remain to be answered, polymer optical waveguides and E-O materials clearly provide an excellent material system for the high-speed photonic applications important to next-generation optical communications.

**Fig. 3.** Optical power spectra at several modulation frequencies. The spectra are shown as wavelength shifts relative to the 1310-nm carrier. The inset shows several microwave frequency modulation sidebands measured with a photodiode. The main figure shows several higher frequency modulation sidebands measured using an optical spectrum analyzer.

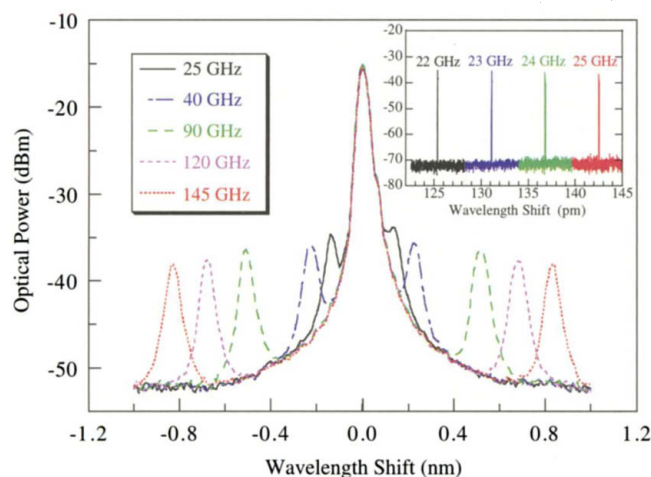
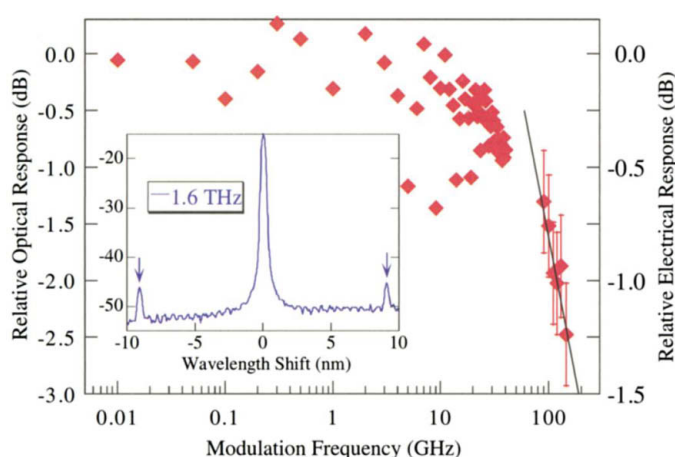


**Fig. 4.** Optical sideband power, normalized to the 10-MHz response, plotted against modulation frequency. The black line indicates the roll-off due solely to electrode surface resistance. The right side scale is the electrical response, which equals the square root of the optical response (14). An optical sideband spectrum at 1.6-THz modulation frequency is shown in the inset.



### References and Notes

1. A. Yariv, *Quantum Electronics* (Wiley, New York, 3rd ed., 1989).
2. C. H. Cox, G. E. Betts, L. M. Johnson, *IEEE Trans. Microwave Theory Tech.* **38**, 501 (1990).
3. W. K. Burns, M. M. Howerton, R. P. Moeller, A. S. Greenblatt, R. W. McElhanon, *IEEE Photon. Technol. Lett.* **10**, 805 (1998).
4. Y. Shi *et al.*, *Science* **288**, 119 (2000).
5. M. Lee, *Appl. Phys. Lett.* **79**, 1342 (2001).
6. C. Zhang, L. R. Dalton, M.-C. Oh, H. Zhang, W. H. Steier, *Chem. Mater.* **13**, 3043 (2001).
7. H. Ma, A. K.-Y. Jen, *Adv. Materials* **13**, 1201 (2001).
8. M. Lee, O. Mitrofanov, H. E. Katz, C. Erben, *Appl. Phys. Lett.* **81**, 1474 (2002).
9. The -3-dB bandwidth is defined as the frequency where the sideband power (at constant  $V_{in}$ ) drops to 0.5, or -3 dB, of its value at a low reference frequency, in this case, 10 MHz. This is equivalent to the -1.5-dB electrical bandwidth.
10. W. Wang *et al.*, *IEEE Photon. Technol. Lett.* **7**, 638 (1995).
11. C. C. Teng, *Appl. Phys. Lett.* **60**, 1538 (1992).
12. D. Chen *et al.*, *Appl. Phys. Lett.* **70**, 3335 (1997).
13. K. Noguchi, O. Mitomi, H. Miyazawa, *J. Lightwave Technol.* **16**, 615 (1998).
14. Materials and Methods are available as supporting material on Science Online.
15. T. A. Tumolillo, P. R. Ashley, *IEEE Photon. Technol. Lett.* **4**, 142 (1992).
16. K. H. Hahn, D. W. Dolfi, R. S. Moshrefzadeh, P. A. Pedersen, C. V. Francis, *Electron. Lett.* **30**, 1220 (1994).
17. The authors thank E. A. Chandross, A. Chowdhury, A. Leven, R. Slusher, and X. Wei for useful discussions and suggestions.

### Supporting Online Material

[www.sciencemag.org/cgi/content/full/298/5597/1401/DC1](http://www.sciencemag.org/cgi/content/full/298/5597/1401/DC1)

Materials and Methods

Conversion Between Optical and Electrical Response

16 August 2002; accepted 17 October 2002